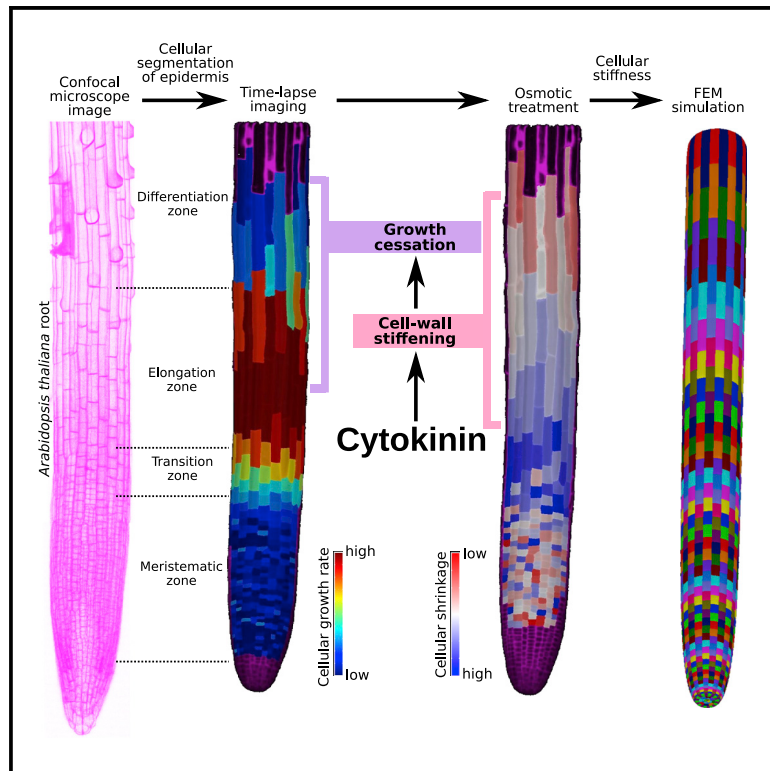# Current Biology

Cytokinin promotes growth cessation in the *Arabidopsis* root

Graphical abstract

Authors
Shanda Liu, Sören Strauss,
Milad Adibi, ..., Peter Huijser,
Richard S. Smith, Miltos Tsiantis

Correspondence
tsiantis@mpipz.mpg.de

In brief

Liu et al. report cell-level growth data from the *A. thaliana* root tip obtained by using live-imaging confocal microscopy. They show that cytokinin promotes growth cessation in the rootward elongation zone, likely through cell wall stiffening in a pathway that also requires the auxin influx transporter AUX1.

Highlights

- Cell-level growth map of the *Arabidopsis* root tip

- Cytokinin promotes growth cessation in the shootward elongation zone

- Growth cessation is associated with cell wall stiffening

- FEM model simulates expansion of cells according to their stiffness and shape

CellPress

Article

Cytokinin promotes growth cessation in the *Arabidopsis* root

Shanda Liu,[1] Sören Strauss,[1] Milad Adibi,[1] Gabriella Mosca,[1,2] Saiko Yoshida,[1] Raffaele Dello Ioio,[3] Adam Runions,[1,7] Tonni Grube Andersen,[4] Guido Grossmann,[5] Peter Huijser,[1] Richard S. Smith,[1,6] and Miltos Tsiantis[1,8,*]

[1]Department of Comparative Development and Genetics, Max Planck Institute for Plant Breeding Research, Carl-von-Linne Weg 10, 50829 Cologne, Germany
[2]Physics Department, Technical University Munich, James-Franck-Str. 1/I, 85748 Garching b. Munich, Germany
[3]Dipartimento di Biologia e Biotecnologie, Laboratory of Functional Genomics and Proteomics of Model Systems, Università di Roma, Sapienza, via dei Sardi, 70, 00185 Rome, Italy
[4]Department of Plant-Microbe Interactions, Max Planck Institute for Plant Breeding Research, Carl-von-Linne Weg 10, 50829 Cologne, Germany
[5]Institute for Cell and Interaction Biology, Heinrich-Heine Universität Düsseldorf, Universitätsstraße 1, 40225 Düsseldorf, Germany
[6]Department of Computational and Systems Biology, John Innes Centre, Norwich NR4 7UH, UK
[7]Present address: Department of Computer Science, University of Calgary, Calgary, AB T2N1N4, Canada
[8]Lead contact
*Correspondence: tsiantis@mpipz.mpg.de
https://doi.org/10.1016/j.cub.2022.03.019

SUMMARY

The *Arabidopsis* root offers good opportunities to investigate how regulated cellular growth shapes different tissues and organs, a key question in developmental biology. Along the root's longitudinal axis, cells sequentially occupy different developmental states. Proliferative meristematic cells give rise to differentiating cells, which rapidly elongate in the elongation zone, then mature and stop growing in the differentiation zone. The phytohormone cytokinin contributes to this zonation by positioning the boundary between the meristem and the elongation zone, called the transition zone. However, the cellular growth profile underlying root zonation is not well understood, and the cellular mechanisms that mediate growth cessation remain unclear. By using time-lapse imaging, genetics, and computational analysis, we analyze the effect of cytokinin on root zonation and cellular growth. We found that cytokinin promotes growth cessation in the distal (shootward) elongation zone in conjunction with accelerating the transition from elongation to differentiation. We estimated cell-wall stiffness by using osmotic treatment experiments and found that cytokinin-mediated growth cessation is associated with cell-wall stiffening and requires the action of an auxin influx carrier, AUX1. Our measurement of growth and cell-wall mechanical properties at a cellular resolution reveal mechanisms via which cytokinin influences cell behavior to shape tissue patterns.

INTRODUCTION

How regulated growth shapes organ forms is a central question in biology. Organ integrity and correct patterning depend on both the initiation and cessation of cellular growth.[1,2] Although the mechanisms that trigger cellular growth are well investigated,[3–5] those that control growth cessation remain less well understood.[6] The *A. thaliana* root offers a powerful system to study this question because of its genetic tractability and ease of imaging.[7,8] Its roots also feature a developmental gradient along their longitudinal axis where cellular growth is triggered, maintained, and eventually terminated.[9–12] How *Arabidopsis* growth is regulated in roots is less well understood than in flowers and leaves, where time-lapse investigations of growth patterns combined with computational modeling have advanced our understanding of how cell-level growth control produces tissue and organ forms.[13–16]

At the proximal (rootward) end of the root tip, the stem cell niche gives rise to the entire root and is maintained by a small group of slowly dividing, auxin-maintained, organizer cells in the quiescent center.[12,17] More distally (shootward) in the meristem, proliferating cells divide and then enter the elongation zone. Here, they stop dividing, grow by elongation,[18] and then stop growing and enter the differentiation zone, where they adopt their final morphology (Figure 1A).[19] A hormonal network involving auxin, cytokinin, brassinosteroids, and ethylene is required for the flexible growth regulation that contributes to root zonation.[20,21] Cytokinin is thought to play a major role in determining the boundary between the meristem and the elongation zone by repressing auxin signaling.[3,22–24]

Plant growth depends on the dynamic regulation of the mechanical properties of the cell wall, which cements cells in place.[25–28] For plant cells to grow, the cell wall must undergo an irreversible expansion in response to turgor pressure.[27] This process depends on cell-wall loosening, mediated by the expansin protein family and other loosening agents.[29] Cell-wall stiffness also influences growth and might modulate the effects of wall loosening.[6,30–32] The role that cell-wall stiffness plays in the spatially distributed control of tissue growth and whether its regulation contributes to growth cessation during development remain to be fully understood.
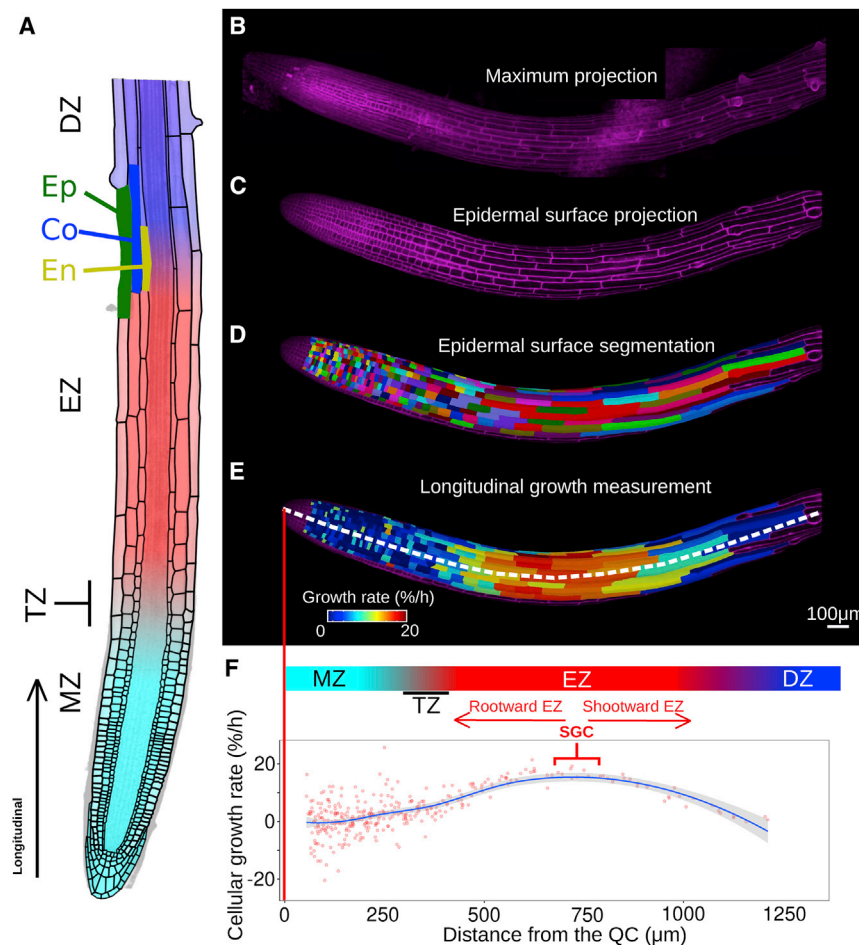
Figure 1. The epidermal cellular growth rate in the *Arabidopsis* root

(A) *Arabidopsis* primary root tip organization along the longitudinal axis: the meristematic zone (MZ, cyan); transition zone (TZ; based on the position of the first elongated cortex cell); elongation zone (EZ; red); and differentiation zone (DZ; dark blue). Cell outlines are shown for the epidermis (Ep), cortex (Co), and endodermis (En).

(B–E) Epidermal cellular growth quantification of a 5 day-after-germination seedling, Col-0 root. (B) Confocal micrograph of a propidium-iodide-stained root in a chambered coverslip with a maximum fluorescence signal projection. (C) Image as described in (B), with the lateral root cap cells removed *in silico* using 3D segmentation to extract the epidermal surface. (D) Surface segmentation. (E) Longitudinal growth rate (cell length measured along the white dashed line) compared with an earlier time point (−1 h). Scale bars, 100 μm.

(F) Plot and schematic of longitudinal root zonation based on cellular growth rate distribution. Data points (red) indicating the cellular growth rate of each epidermal cell and the trend line (blue) with 95% confidence intervals (shaded area). The start of growth cessation (SGC) is highlighted.

See also Figures S1 and S2.

We investigated the morphogenetic basis for growth cessation in the elongation zone by capturing cellular growth profiles along the root longitudinal axis. We found that cytokinin induces growth cessation. Through osmotic-treatment-based measurements of cell-wall stiffness and computational modeling, we show that cytokinin-mediated growth cessation is associated with an increase in cell-wall stiffness in the elongation zone. Our results show that these cytokinin effects require the action of the auxin efflux carrier AUX1, which increases auxin activity in the elongation zone. Together, our data illustrate how quantitative analyses of cellular growth and cell-wall stiffness can uncover how hormone-dependent genetic regulation influences cell-level properties to shape root tissue patterning. They also provide cell-level growth distribution information that should further inform computational modeling studies of root development and tissue zonation.[12,42,43]

RESULTS

Cytokinin promotes growth cessation in the elongation zone

In plant roots, the hormone cytokinin regulates growth and differentiation[5,22,33–37] and promotes cell exit from the meristem and the onset of differentiation. When two type B ARR (*Arabidopsis* response regulator) transcription factors, ARR1 and ARR12 (which mediate cytokinin signaling), are knocked out, the root and root meristems become longer.[22] Conversely, when cytokinin levels are increased, root growth is inhibited, and precocious differentiation reduces the meristem's size.[22,35,37] These studies show that cytokinin regulates root morphology and development at the organ level but how it controls the distribution of cell-level growth in space and time is less clear. Kinematic and computational studies of root growth have investigated the genetic network that controls root growth and zonation.[20,21,38] These studies alongside investigations of growth control in the shoot indicate that genetic control probably regulates plant form and growth by controlling cell mechanics during symplastic growth.[21,30] Existing growth analysis methods mainly track particles or matched pixels on image series acquired from microscopes. These approaches provide valuable insights into the longitudinal root growth profile and its control.[39–41] An alternate approach we develop here is to use segmented surface projections obtained using confocal microscopy time-lapse imaging to measure the expansion of individual cells over time. This allows us to directly associate cell-level changes in mechanical properties with changes in growth.[6,30]

To study the cellular growth rate distribution along the root longitudinal axis, we used live-imaging confocal microscopy and a previously described chambered coverslip system.[44,45] We first verified that root morphology in this system is quantitatively similar to that of plants grown on a widely used agar plate system (Figure S1).[36,46] We conducted time-lapse experiments on 5-day-after-germination seedlings, captured root images at cellular resolution, and used MorphoGraphX to segment the epidermal cells from surface projections and to measure the
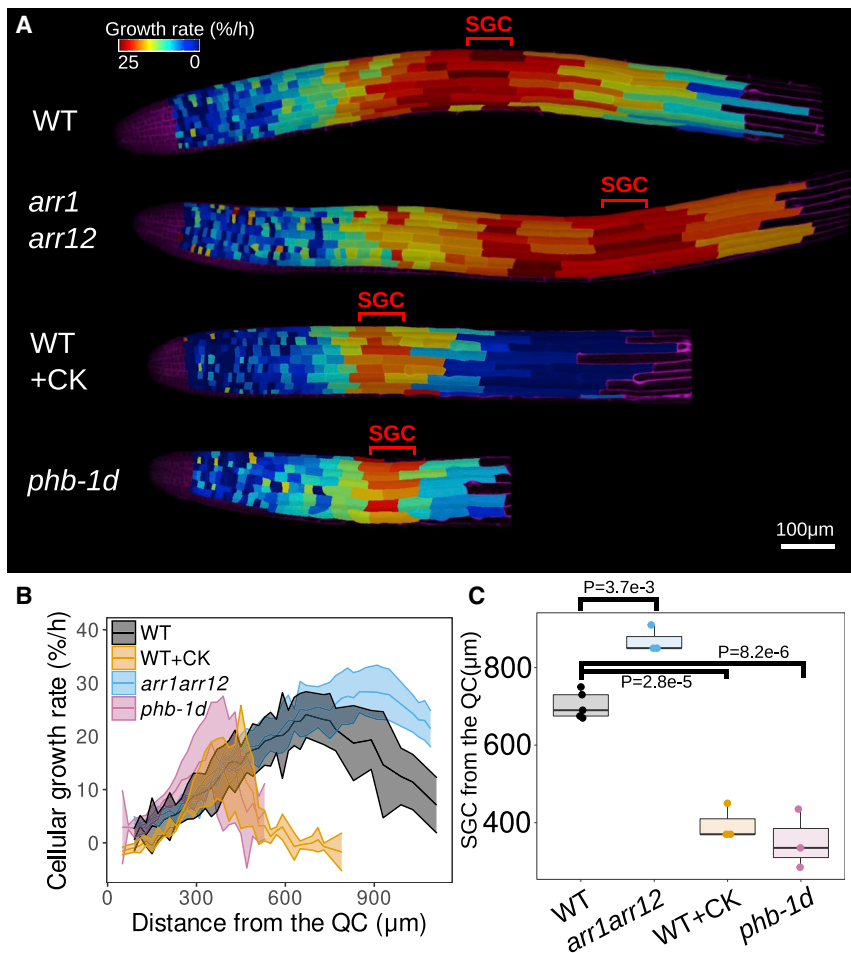
Figure 2. Changes in cytokinin activity alter cellular growth cessation in the elongation zone

(A) Cellular growth rates in 5-day-after-germination (DAG) seedlings of the WT, *arr1arr12*, *phb-1d*, and WT roots treated for 23 h with cytokinin (1 μM *trans*-zeatin, tZ). Heatmaps show a 1-h relative cell growth rate along the longitudinal axis compared with an earlier time point. The start of growth cessation (SGC) points are highlighted. Similar patterns were observed in 3–5 replicates; one representative example for each group is shown. The roots were imaged in chambered coverslips stained with propidium iodide. Scale bars, 100 μm.

(B) Cellular growth profiles in the 5DAG WT (n = 5), *arr1arr12* (n = 3), *phb-1d* (n = 3), and WT roots treated for 23 h with cytokinin (1 μM tZ) (n = 3). The shaded regions correspond to the standard deviation.

(C) SGC comparisons for root genotypes, treatments, and n, as described in (B). The data were analyzed by a one-way ANOVA and Tukey's honestly significant difference (HSD). Error bars represent standard deviation, p values < 0.01. See also Figure S4.

phb-1d mutant, in which cytokinin biosynthesis is enhanced;[36] and the cytokinin-treated roots (Figures 2A and 2B). In WT roots, the cessation of growth starts at ~700 μm from the quiescent center. In *arr1arr12* double-mutant roots, growth cessation is delayed relative to that in WT—starting at ~850 μm. In the cytokinin-treated WT and *phb-1d* roots, growth cessation starts spatially earlier than that in WT—between 300 and 400 μm (Figure 2C). Similar trends were also seen when comparing the number of epidermal cells from the quiescent center to the SGC (Figure S4B). In the cytokinin-treated WT and *phb-1d* roots, the SGC was reached at a lower cell number from the quiescent center (between 20 and 25) relative to that in WT (~30), whereas in *arr1arr12* double mutants, the SGC was reached after a higher cell number from the quiescent center (~35; Figure S4B). Thus, cytokinin reduces both the number of cells and the distance between the quiescent center and the SGC, which includes the meristem and the rootward elongation zone. This result is consistent with that of previous work reporting smaller meristem sizes in cytokinin-treated roots.[22] In summary, our results indicate that reduced cytokinin signaling delayed growth cessation, whereas increased cytokinin levels promoted it precociously. They also suggest that growth cessation is promoted by cytokinin during the transition to differentiation and might result from a gradual effect that becomes apparent in the transition zone and the elongation/differentiation zone.

Cytokinin accelerates cell-wall stiffening in the shootward elongation zone

Next, we investigated whether cytokinin could promote growth cessation by changing cell-wall mechanical properties, in particular stiffness, in the elongation zone. To do so, we
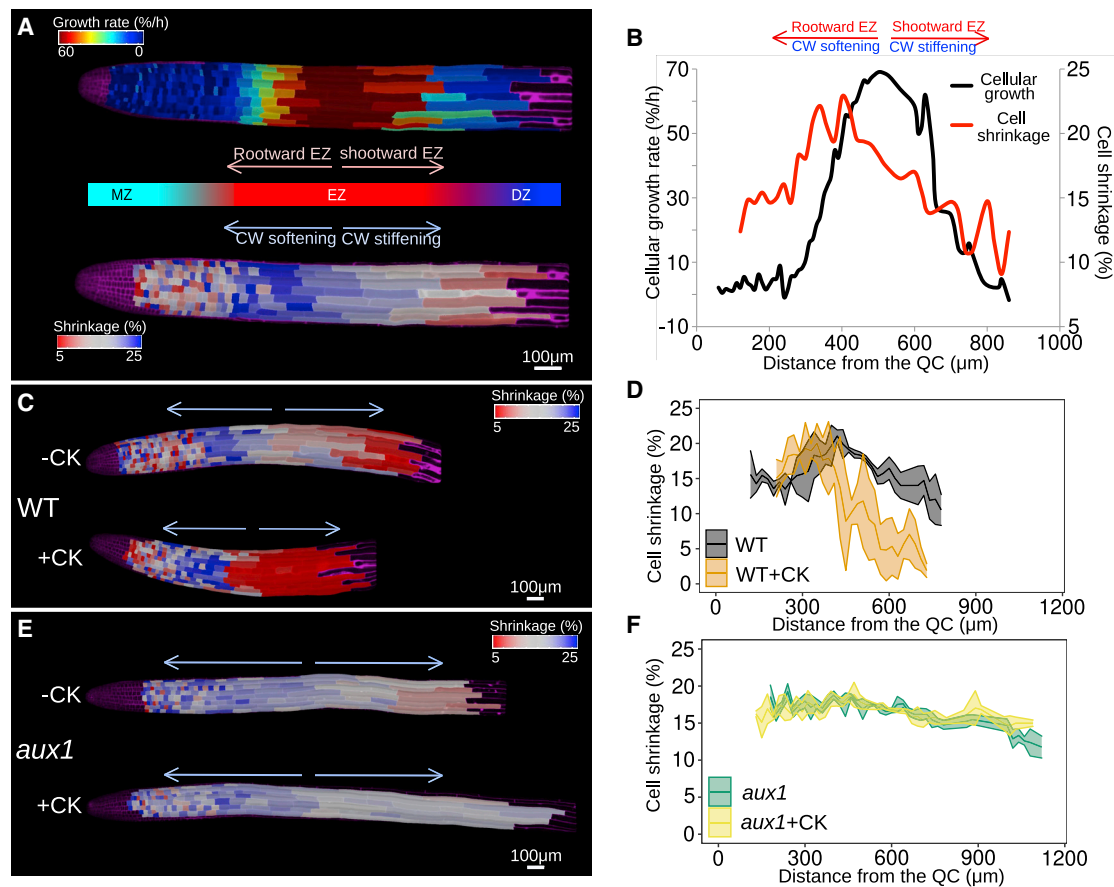
cellular growth rates (Figures 1B–1F).[47] In the tip of the wild-type (WT) roots, the cellular growth rate gradually increased as cells moved away from the quiescent center and reached its maximum at ~700 μm from the quiescent center. The growth rate then gradually decreased as the cells moved further away from the quiescent center (Figures 1E and 1F). We defined the position at which the cellular growth rate began to decrease as the start of growth cessation (SGC) occurs, thus dividing the elongation zone into two sub-domains: the rootward elongation zone and the shootward elongation zone (Figure 1F). This is consistent with observations in previous kinematic studies.[39–41] We used the distance between the quiescent center and the SGC to compare the growth cessation activity in different genotypes and treatments. The root growth profile acquired using cell-level measurements provided a broadly similar distribution to that previously reported using kinematic analyses and added cellular resolution.[39–41]

From the cell-level measurements, we extracted the distance and the number of epidermal cells from the quiescent center to the SGC—both of which are commonly used measurements for evaluating root meristem size and longitudinal root zonation.[22,48] To investigate how cytokinin controls cell-level growth in roots, we compared roots from: WT (Col-0) plants; the *arr1arr12* double mutant (*arr1-3 arr12-1*), in which cytokinin signaling is reduced; the

Figure 3. Cytokinin accelerates cell-wall stiffening in the shootward elongation zone through AUX1

(A) (Upper) Heatmap of longitudinal percentage cellular growth rate for a 5-day-after-germination (DAG) WT root, relative to an earlier time point (−1 h). (Lower) Heatmap of longitudinal percentage cellular shrinkage for the same root following osmotic treatment, relative to a +1 h time point.

(B) Longitudinal cellular growth rate (black) and cell shrinkage (red) distribution for the root shown in (A). Similar patterns were observed in 3 replicates from independent experiments, one representative example is shown.

(C and E) Osmotic treatment cell-shrinkage heatmaps in 5DAG WT and *aux1-10* mutant roots in the presence and absence of cytokinin (6 h 1 μM tZ). The linear color bar indicates the percentage of cell shrinkage upon osmotic treatment. For each group, similar patterns were observed in three replicates and one representative sample is shown.

(D and F) Cell-shrinkage distribution along the longitudinal axis of osmosis-treated 5DAG WT and *aux1-10*-mutant roots in the presence and absence of cytokinin (6 h 1 μM tZ). The shaded regions correspond to the standard deviation. n = 3 for each genotype. The roots were imaged in the RootChip stained with propidium iodide. Scale bars, 100 μm.

See also Figure S2.

estimated cell-wall stiffness distribution in roots by measuring cellular shrinkage in response to a hyperosmotic solution, which causes cells to shrink due to loss of turgor pressure.[49] This assay is used to estimate cell-wall stiffness in plant tissues[30,31,49] because the degree of cellular shrinkage on treatment correlates negatively with cell-wall stiffness. Here, we adapted this method for a microfluidic device, the RootChip, to apply the hyperosmotic solution with minimal interference.[50,51] We first examined the distribution of relative cell shrinkage longitudinally (shrinkage in length) in WT roots following osmotic treatment to test how this shrinkage correlates with cellular growth rate. As with growth, shrinkage along the longitudinal direction is the same in all cell layers as they are physically linked. Length shrinkage in the meristem was ~15% and reached a maximum of ~22% in the rootward elongation zone (around 400 μm from the quiescent

center), followed by a rapid increase in cellular growth rate in the elongation zone (Figures 3A and 3B; Video S1). In the shootward elongation zone, shrinkage in length gradually decreased, followed by an increase in growth cessation (Figures 3A and 3B). Based on the premise that reduced longitudinal cell shrinkage in the elongation zone in response to osmotic treatment indicates a change in cell-wall stiffness, these results suggest that growth cessation in the shootward elongation zone is caused by increased cell-wall stiffness along the longitudinal axis. Although this premise is valid, cell geometry and arrangement also affect physical forces, which in turn influence cellular responses to osmotic treatment.[32,52] In the *Arabidopsis* root, cell length in the elongation zone increases along the longitudinal axis due to rapid cell expansion (Figure S2A). Thus, the longitudinal cell-shrinkage gradient we measured following osmotic
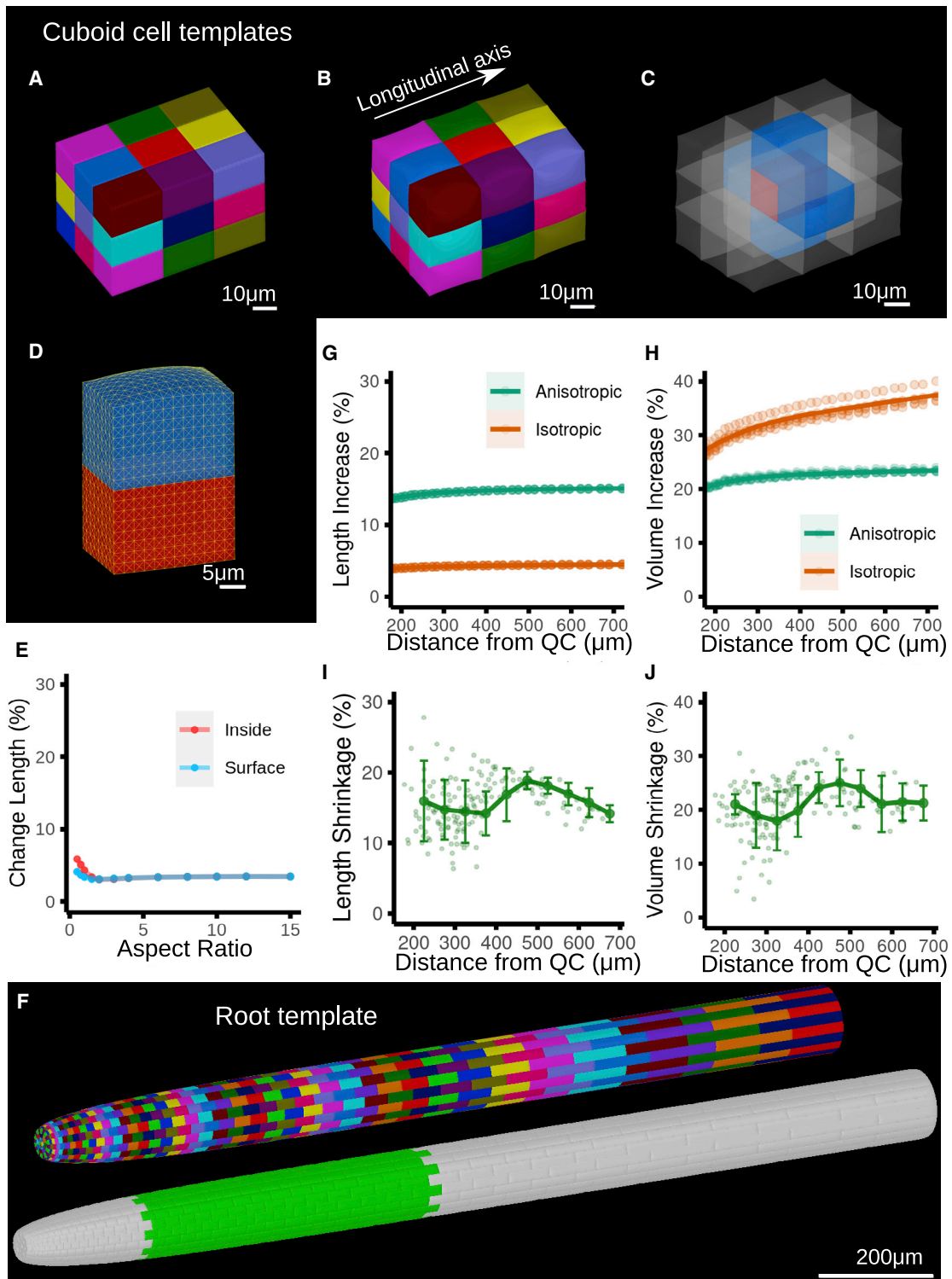
Figure 4. Cell geometry influence on mechanical properties in the root epidermis

(A–E) Pressurization simulations using 3 × 3 blocks of cuboid cells. (A–D) Block of cells (width and depth, 16 μm; length, 24 μm; aspect ratio, 1.5) (A) before and (B) after pressurization. (C) Due to the bulging of cell walls at the surface, only the cells with unexposed front and back walls in the longitudinal direction were analyzed, resulting in 2 cell types: one inside cell (red) and four surface cells (blue) (Video S2).[32] (D) Surface cells (blue) bulge after pressurization. (E) Quantification of cell-length change on pressurization of template in (A).

(legend continued on next page)

treatment could be partially explained by changes in cell geometry and arrangement rather than by a tissue-level gradient in cell-wall material properties.

To evaluate this possibility, we simulated the effect of turgor pressure on the elastic expansion of cells using the finite element method (FEM) implemented in the MorphoMechanX software (Video S2).[32,53] Previous studies indicate that increased cell length alone is unlikely to influence mechanical stress along the longitudinal direction and therefore cell expansion.[52] To verify this prediction for root cells and to integrate the effect of tissue context, we explored the influence of cell length on two different templates: one consisting of rectangular cuboid cells of varying aspect ratio (length/width) arranged in blocks (Figures 4A–4D) and the other consisting of epidermal-like cells arranged in a hollow cylinder (Figures S3A and S3B). We then measured the increase in cell length after *in silico* pressurization of these templates.[47,53,54] In both, the pressure-induced deformation of cell length remained constant at ∼4% for cells with an aspect ratio >2 (Figures 4E and S3E). These observations support the view that increased cell length alone is unlikely to affect osmotic-treatment-induced deformation along the longitudinal axis.[52]

The *Arabidopsis* primary root tip has more complex cell shapes and arrangements than those represented in these two templates. Therefore, we created an idealized root template composed of several cell layers based on cell-size measurements obtained from 3D root images (Figure 4F). We initially assumed isotropic cell-wall properties, as in previous simulations (Table S1).[32] In this template, the pressurization-induced change in cell length was the lowest at the tip and increased slightly in the meristem where the root widens but then remained relatively constant at ∼5% in the elongation and differentiation zone where cell length dramatically increased (Figures 4G and S2A). These results confirm that the cell-length distribution along the longitudinal axis has very little impact on pressure-induced cell-length deformation. Therefore, our osmotic treatment experimental results (where cell shrinkage depended on the distance from the quiescent center; Figure 3B) cannot be explained by a change in cell geometry alone (see Video S3 for a comparison of osmotic treatment and simulation). Instead, changes in cell-wall properties are likely the predominant driver for the decrease in osmotic-induced cell-length shrinkage in the shootward elongation zone.

Next, we conducted a quantitative comparison of the simulation and experimental data to assess how well our isotropic-material simulations reflected the osmotic-treatment-induced deformation in 3D. We segmented root epidermal cells in 3D before and after osmotic treatment *in silico* and quantified how their geometry changed. Within the elongation zone, the simulation showed a higher volume change (between 25% and 40%) compared with the experiment (around 20%; compare Figures 4H and 4J), whereas the length change was considerably lower (5% in the simulation compared with 10%–20% in the experiment; compare Figures 4G and 4I). These differences suggest that simulations using isotropic cell-wall materials are not sufficient to match the cell length and volume deformation that occur in the osmotic treatment. Previous work in the shoot has indicated that fast-growing areas display more elastic cell walls relative to slow-growing areas.[6,30] Furthermore, the cortical microtubules that guide cellulose microfibril deposition, the main load-bearing components of the cell wall,[55] are highly transversal in the elongation zone of *Arabidopsis* roots.[56] Therefore, cell walls might be softer along the longitudinal axis. In the last simulation, we used such anisotropic cell-wall materials and obtained a higher convergence of experimental and simulation results (Figures 4G–4J; Table S1),[57] which is consistent with the idea that the cell-wall material in the root is highly anisotropic and of lower stiffness along the longitudinal axis than along other axes.

Overall, our findings indicate that cell-length shrinkage in the shootward elongation zone in response to osmotic treatment is unlikely to reflect changes in cell shape and arrangement (Figures 3A and 3B) but instead changes in cell-wall stiffness. Given this, we compared the distribution of cell shrinkage in the elongation zone in the presence and absence of cytokinin treatment (6 h 1 μM *trans*-zeatin [tZ]). Cytokinin-treated roots had a greater decrease in cell shrinkage in the shootward elongation zone relative to the untreated WT roots (Figures 3C and 3D; Video S1), suggesting that cytokinin-mediated growth cessation in the shootward elongation zone involves cell-wall stiffening.

AUX1 is required for cytokinin-induced cell-wall stiffening and growth cessation in the elongation zone

Having obtained evidence that cytokinin promotes growth cessation by modulating cell-wall stiffness in the shootward elongation zone, we next looked for possible cytokinin effectors in this process. One candidate regulator is the auxin influx carrier AUX1.[58–60] AUX1 acts as a positive regulator of root growth in response to cytokinin, and the *aux1* loss-of-function mutant roots are insensitive to cytokinin treatment.[37] Thus, we hypothesized that AUX1 might be required for both cytokinin-induced cell-wall stiffening and growth cessation. To test this, we compared the effect of cytokinin on cell-wall stiffness in the AUX1 loss-of-function mutant, *aux1-10*. The exogenously applied cytokinin (6 h 1 μM tZ) affected cell-wall stiffness distribution in the WT roots (500–800 μm from the quiescent center), but not in the *aux1-10* mutant roots (Figures 3C–3F; Video S1).

(F–H) Simulations using an artificial root template. (F) Root template before (top, cell label colors) and after (bottom) pressurization using anisotropic cell-wall properties. The cell sizes were obtained from real root cell measurements. Green indicates the region between 200 and 700 μm from the quiescent center, which was compared with experimental data (Video S3). (G and H) The change of cell length and volume in the epidermis cells of model template in (F) on pressurization using isotropic and anisotropic cell-wall material. Only data between 200 and 700 μm are shown. Data points in the plots refer to individual cells, and trends are shown with a fitting line (see Figures S3H and S3I for all data points 0–1,500 μm).

(I and J) Quantification of cell length and volume shrinkage after osmotic treatment, relative to before, measured in 3D segmented cells (compare I with G and J with H). Raw data points are shown for each cell, together with their mean values of 50 μm bins in a darker color. Error bars represent the standard deviation of the bin.

Scale bars: 10 μm in (A–C), 5 μm in (D), and 200 μm in (F).
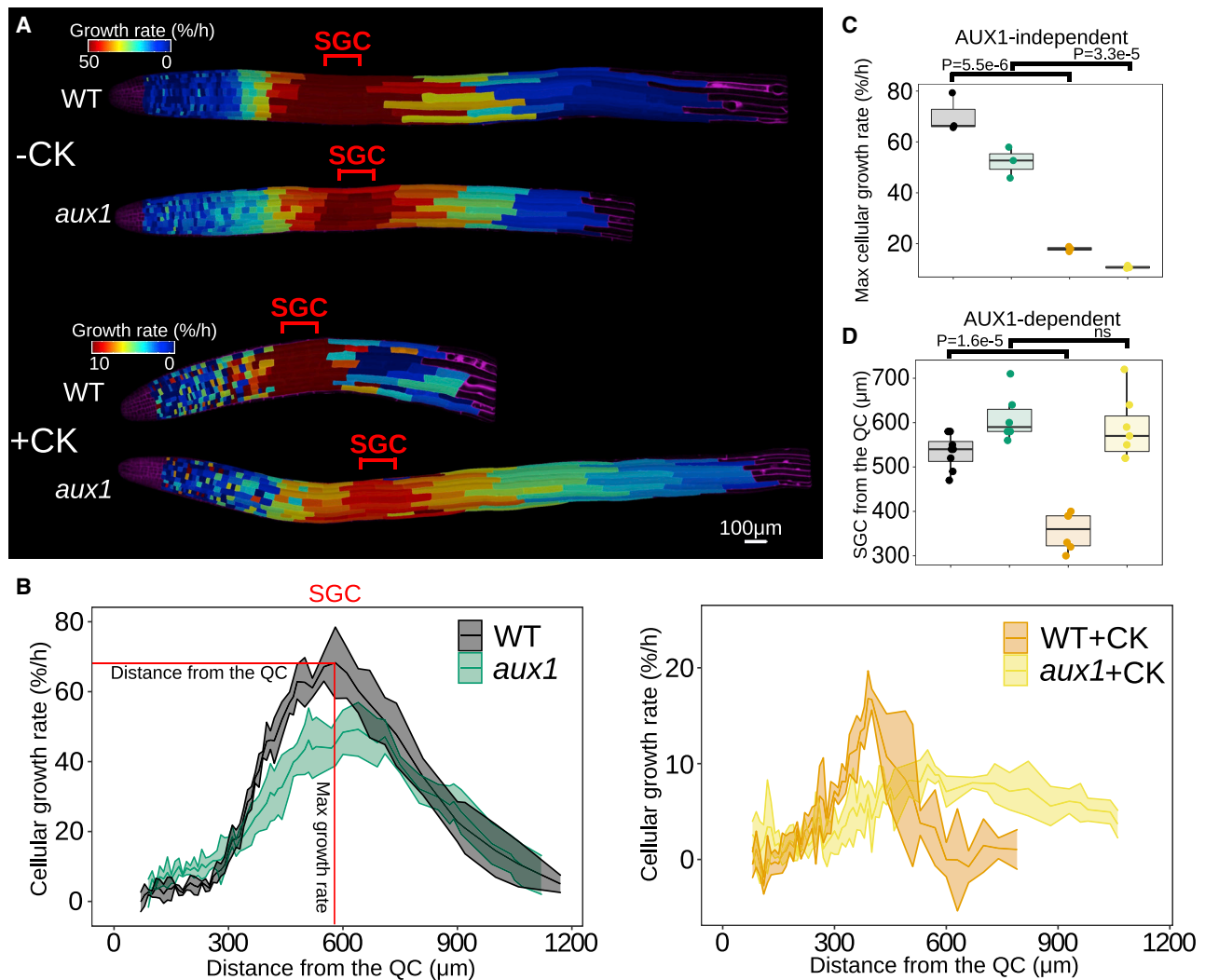
See also Figure S3 and Table S1.

Figure 5. AUX1 is required for cytokinin-induced growth cessation in the elongation zone

(A) Heatmaps of longitudinal cellular growth rate in 5-day-after-germination seedlings of WT and *aux1-10* mutant roots in the presence or absence of cytokinin (6 h 1 μM tZ). The start of growth cessation (SGC) locations are highlighted. Similar patterns were observed in 3 replicates, one representative example for each group is shown. The roots were imaged in the RootChip and stained with propidium iodide. Scale bars, 100 μm.

(B) Cellular growth rate profiles for the WT and *aux1-10* mutant in the presence or absence of cytokinin (6 h 1 μM tZ). The shaded regions correspond to the standard deviation. n = 3 for each genotype.

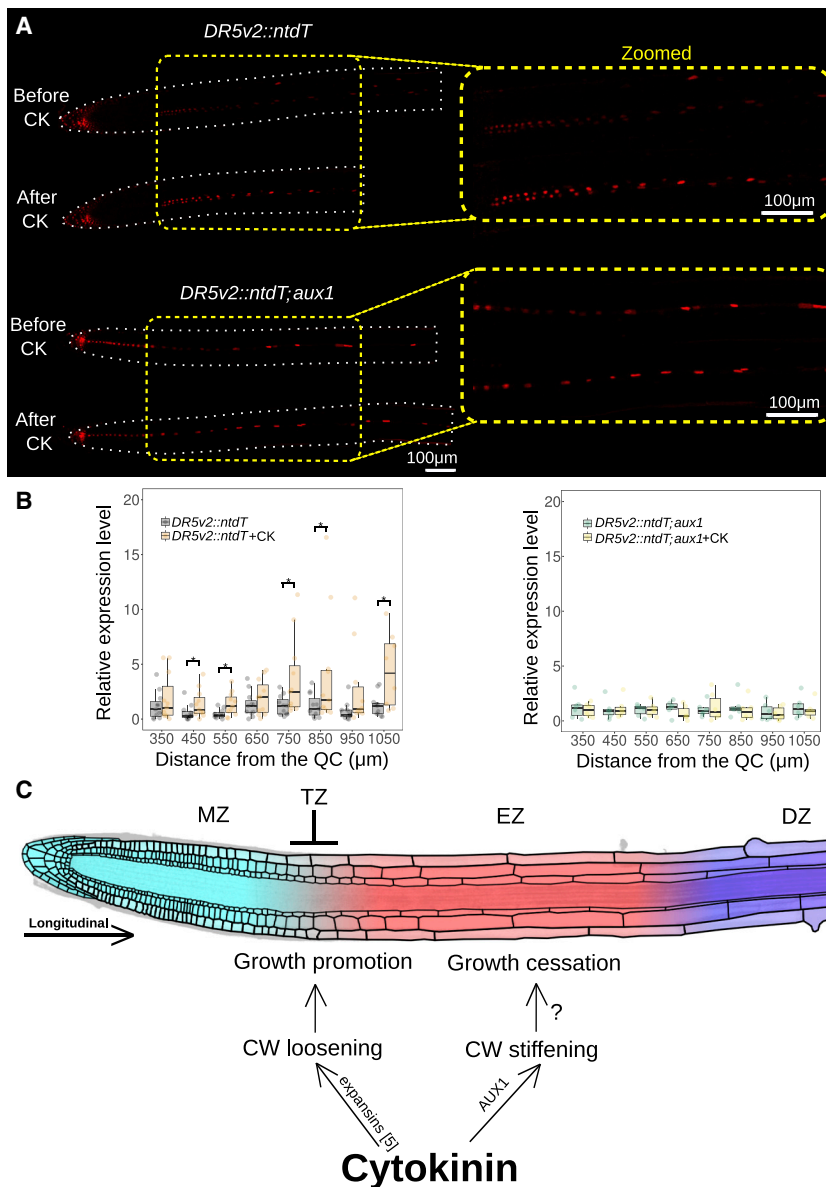(C) Maximum cellular growth rate in the elongation zone as in (B).

(D) Quantification of distance from the quiescent center to the SGC, n = 8, 6, 6, and 7.

Data in (C and D) were analyzed by a one-way ANOVA and Tukey's HSD. The error bars represent the standard deviation, p values < 0.01.

These results suggest that cytokinin-induced cell-wall stiffening in the shootward elongation zone is AUX1-dependent, although the underlying molecular mechanism needs further investigation.

Our results indicate that cytokinin-induced cell-wall stiffening might cause the cessation of cell growth in the shootward elongation zone. Since the *aux1-10* mutant is insensitive to exogenous cytokinin, we reasoned that this mutant should also be insensitive to cytokinin-induced growth cessation (if AUX1-mediated cell-wall stiffening is functionally important for growth cessation). To test this hypothesis, we compared the effect of exogenous cytokinin on growth cessation in the WT and *aux1-10* mutants. The cytokinin treatment (6 h 1 μM tZ) was sufficient to accelerate

growth cessation in the WT roots, but not in the *aux1-10* mutants (Figures 5A and 5B). In the absence of cytokinin, the distance from the SGC to the quiescent center was 540 μm in the WT—this was reduced to ~360 μm after the cytokinin treatment. For the *aux1-10* mutants, we measured a distance of ~580 μm in the absence of cytokinin, which remained at ~550 μm after cytokinin treatment (Figure 5D). These results indicate that the *aux1-10* mutants are insensitive to cytokinin-induced cell-wall stiffening and cytokinin-induced growth cessation in the shootward elongation zone. This is consistent with the hypothesis that cytokinin promotes growth cessation by modulating cell-wall stiffness in the shootward elongation zone through AUX1.

Figure 6. Cytokinin upregulates auxin activity in the stele of the elongation zone and a model of cytokinin regulating root cell growth

(A) *DR5v2::ntdTomato* (*DR5v2::ntdT*) reporter activity in 5-day-after-germination seedling roots in the presence or absence of cytokinin (6 h 1 μM tZ) (upper, WT; lower, *aux1-10* mutant). (Left) Longitudinal cross-sections of the roots; organ boundaries are marked by white dashed lines. (Right) Magnified images of *DR5v2::ntdTomato* expression in the stele, as highlighted by the yellow box. Similar patterns were observed in 9 out of 11 replicates for the WT and in 5 out of 6 replicates for the *aux1-10* mutants. The roots were imaged in the RootChip. Scale bars, 100 μm.

(B) Changes in *DR5v2::ntdTomato* expression in response to cytokinin treatment in the stele. Raw expression data were extracted from the 3D image stack and binned (bin size = 100 μm) in the 3D space along a manually placed curve along the longitudinal axis at the root center. The expression level was normalized by comparing the raw expression value in each bin to the average bin expression value of the sample before treatment. Data points indicate the normalized relative expression level of a bin in a sample. n = 11 for the WT and n = 6 for the *aux1-10* experiments. The data were analyzed with the Student's t test. Error bars represent the standard deviation, *p < 0.05.

(C) The roles of cytokinin in regulating cell-level growth at the transition zone (TZ) and elongation zone (EZ). In this model, cytokinin promotes growth at the transition zone by loosening the cell wall via expansins, thus establishing the meristem/transition zone boundary.[5] In the shootward elongation zone, cytokinin likely promotes growth cessation by stiffening the cell wall through AUX1, possibly by modulating auxin activity.

Cytokinin promotes auxin signaling in the elongation zone

If cytokinin-induced cell-wall stiffening and growth cessation in the shootward elongation zone requires AUX1, then how is auxin homeostasis involved in these processes? During root gravistimulation, an auxin-signaling maximum is created at the lower side of the root. This induces cell-wall alkalization, which leads to local growth inhibition and the downward bending of roots.[4,61] Thus, we hypothesized that cytokinin may promote growth cessation in the elongation zone by increasing auxin activity through AUX1.

To test this hypothesis, we analyzed the effect of exogenously applied cytokinin on auxin signaling in the elongation zone of the WT and *aux1* mutants by monitoring the expression of *DR5v2::ntdTomato*, an auxin response reporter line.[62] Cytokinin treatment (6 h 1 μM tZ) substantially induced *DR5v2::ntdTomato* expression in the stele of elongation and differentiation zones (450–1,050 μm from the quiescent center) in WT, but not in the *aux1-10* mutant (Figures 6A and 6B). In most of the WT background roots, *DR5v2::ntdTomato* was expressed in the lateral root cap and in the stele of the elongation

Although the *aux1-10* mutant is insensitive to cytokinin-induced cell-wall stiffening and growth cessation in the shootward elongation zone, it remains partially sensitive to cytokinin-mediated growth inhibition. To test whether AUX1-independent processes also mediate the effects of cytokinin on growth in the elongation zone, we measured the maximum cellular growth rate as an indicator of overall cellular growth activity in this domain (Figure 5B). After the cytokinin treatment (6 h 1 μM tZ), the maximum cellular growth rate in the WT roots was inhibited from 70% to 17% (per h), signifying an ∼75% reduction. Similarly, the cellular growth rate was reduced in the *aux1-10* mutant by 80% after cytokinin treatment (Figure 5C). These results indicate that cytokinin inhibits cellular growth in the entire elongation zone through AUX1-independent processes, in addition to promoting growth cessation by modulating cell-wall stiffness in the shootward elongation zone through AUX1.

and differentiation zones (9/11; Figure 6A). In most of the *aux1-10* plants, *DR5v2::ntdTomato* was expressed in the same domains with additional expression in the stele of the meristematic zone (5/6; Figure 6A). These results suggest that cytokinin promotes auxin activity in the stele of the elongation zone, partly through AUX1. Notably, in the *aux1-10* mutant, despite cell-wall stiffness distribution being insensitive to exogenous cytokinin, the cellular growth rate was inhibited in both the shootward and rootward elongation zone, similar to that in WT (Figures 3C–3F and 5C). This suggests that cytokinin might repress cellular growth more broadly through AUX1-independent processes, in addition to terminating cellular growth in the shootward elongation zone.

DISCUSSION

Despite considerable progress in understanding the genetics of root development, the cell-level processes that determine growth cessation and the physical basis of growth regulation remain poorly understood. Here, by using cell-level measurements and computational analyses, we identify a role for cytokinin in growth cessation in the shootward elongation zone (Figure 2) as well as cell-wall mechanical changes that likely underpin this growth regulation (Figures 3A–3D). Additionally, we provide evidence that this cytokinin action involves an AUX1-dependent increase in auxin activity in the stele of the elongation zone (Figures 3C–3F, 5, and 6). As AUX1 plays a key role in auxin transport, reduced AUX1 levels[37] might cause less auxin to be transported from the elongation zone toward the root tip, leading to increased auxin activity in the elongation zone. It is possible that increased AUX1 activity in the stele acts indirectly on the longitudinal growth of the entire root, as recently shown in the case of brassinosteroids and tissue-specific rescue of the *bri1* mutant.[63]

Previous models have explored how growth cessation might be controlled.[21,64] Pavelescu et al. analyzed kinematic data for roots deficient in brassinosteroids and gibberellic acid signaling; both require a significant reduction in the cell elongation rate in the elongation zone to fit the kinematic data.[64] Our results suggest a parallel role for cytokinin and demonstrate stiffness changes that result in reduced growth throughout the elongation zone (compare Figures 2B and 3D). De Vos et al. note that symplastic growth requires a certain amount of spatial coordination to maintain stable growth and suggest that cytokinin might flatten auxin gradients to make growth more uniform.[21] This idea is consistent with our observations that cytokinin broadly affects root growth (Figures 2 and 5). Future work will need to determine the specific tissue layers that are required for cytokinin-mediated growth control.[65–68] However, because layers must grow in synchrony during development to avoid tissue tearing, determining the primacy of external versus internal layers as "growth controllers" will be non-trivial to address.

Prior work indicates that cytokinin regulates root zonation by positioning the transition zone,[5,69] possibly via the expansin-dependent acidification of the apoplast and consequent cell-wall loosening and growth increase (Figure 6C).[5] This idea implies that cytokinin action is context-specific as it promotes growth at the transition zone when cells exit the meristem while contributing to growth arrest more distally. Other domain-

specific cofactors, such as auxin activity gradients, might account for this dual role. Because the extensibility and stiffness of the cell wall are biophysically distinct processes,[27,29] this context-dependent role might reflect the engagement of cytokinin with these two aspects of growth control, which would also provide opportunities to homeostatically regulate growth. As cytokinin appears to promote differentiation,[22,42] the cell-wall stiffening associated with growth cessation might be due to differentiation. Stiffening beyond a threshold might override the capacity of extensibility to cause further growth. During the transition from elongation to differentiation, cytokinin promotes the reorganization of the cortical microtubule array,[56,70] which delivers and deposits new cell-wall components.[55] Thus, the cytokinin-induced cell-wall stiffening reported here might be mediated by modulated microtubule dynamics.

In summary, we propose that cytokinin has two distinct roles in promoting root differentiation: (1) increased growth, accompanying the passage from the meristem into the faster growing transition zone[5] (Figure 6C) and (2) repressed growth in the shootward elongation zone, which causes growth cessation (Figure 6C). Future work will need to test these ideas by examining cell-level growth and cell-wall properties in different mutants and transgenic lines in which relevant root gene regulatory network components and cell-wall regulators are perturbed.[5,31,56,71] Such work will require further advances in biophysics methodologies and computational modeling frameworks[72] and will enable us to explore how the regulation of stiffness and extensibility affects growth at different developmental stages. As cytokinin has multiple roles in shoot organ development,[73–75] it will be interesting to explore whether its regulation of wall stiffness also mediates some of its effects in the shoot. Overall, our work illustrates how cell-level, image-based growth analysis—combined with the studies of cell-wall properties and computational simulations—can provide a multi-scale understanding of the genetic processes shaping plant form.

STAR★METHODS

Detailed methods are provided in the online version of this paper and include the following:

- KEY RESOURCES TABLE
- RESOURCE AVAILABILITY
  - Lead contact
  - Material availability
  - Data and code availability
- EXPERIMENTAL MODEL AND SUBJECT DETAILS
  - Plant materials and growth conditions
- METHOD DETAILS
  - Hormonal and osmotic treatments
  - Microscopy and image analysis with MorphoGraphX
  - Computational simulations
- QUANTIFICATION AND STATISTICAL ANALYSIS

SUPPLEMENTAL INFORMATION

Supplemental information can be found online at https://doi.org/10.1016/j.cub.2022.03.019.

AUTHOR CONTRIBUTIONS

S.L., M.A., R.D.I., R.S.S., and M.T. designed the experiments; S.L. performed the majority of the experiments and analyses; S.S. conducted the computational simulations with input from G.M. and A.R.; S.L. and S.S. prepared the figures; S.Y. and P.H. contributed to the imaging; R.D.I. contributed materials and imaging; G.G. helped establish the RootChip system and provided the devices; T.G.A. contributed to image acquisition; S.L., S.S., and M.T. wrote the manuscript with input from other authors, particularly G.M., A.R., and R.S.S.; and M.T. directed the study.

DECLARATION OF INTERESTS

The authors declare no competing interests.

REFERENCES

1. Stieper, B.C., Kupershtok, M., Driscoll, M.V., and Shingleton, A.W. (2008). Imaginal discs regulate developmental timing in *Drosophila melanogaster*. Dev. Biol. *321*, 18–26. https://doi.org/10.1016/j.ydbio.2008.05.556.

2. Averbukh, I., Ben-Zvi, D., Mishra, S., and Barkai, N. (2014). Scaling morphogen gradients during tissue growth by a cell division rule. Development *141*, 2150–2156. https://doi.org/10.1242/dev.107011.

3. Moubayidin, L., Perilli, S., Dello Ioio, R., Di Mambro, R., Costantino, P., and Sabatini, S. (2010). The rate of cell differentiation controls the *Arabidopsis* root meristem growth phase. Curr. Biol. *20*, 1138–1143. https://doi.org/10.1016/j.cub.2010.05.035.

4. Barbez, E., Dünser, K., Gaidora, A., Lendl, T., and Busch, W. (2017). Auxin steers root cell expansion via apoplastic pH regulation in *Arabidopsis thaliana*. Proc. Natl. Acad. Sci. USA *114*, E4884–E4893. https://doi.org/10.1073/pnas.1613499114.

5. Pacifici, E., Di Mambro, R., Dello Ioio, R., Costantino, P., and Sabatini, S. (2018). Acidic cell elongation drives cell differentiation in the *Arabidopsis* root. EMBO J. *37*, e99134. https://doi.org/10.15252/embj.201899134.

6. Hong, L., DuMond, M., Tsugawa, S., Sapala, A., Routier-Kierzkowska, A.L., Zhou, Y., Chen, C., Kiss, A., Zhu, M., Hamant, O., et al. (2016). Variable cell growth yields reproducible OrganDevelopment through spatiotemporal averaging. Dev. Cell *38*, 15–32. https://doi.org/10.1016/j.devcel.2016.06.016.

7. Dolan, L., Janmaat, K., Willemsen, V., Linstead, P., Poethig, S., Roberts, K., and Scheres, B. (1993). Cellular organisation of the Arabidopsis thaliana root. Development *119*, 71–84.

8. Benfey, P.N., and Scheres, B. (2000). Root development. Curr. Biol. *10*, R813–R815. https://doi.org/10.1016/S0960-9822(00)00814-9.

9. Scheres, B., Benfey, P., and Dolan, L. (2002). Root development. Arabidopsis Book *1*, e0101. https://doi.org/10.1199/tab.0101.

10. Salvi, E., Di Mambro, R., and Sabatini, S. (2020). Dissecting mechanisms in root growth from the transition zone perspective. J. Exp. Bot. *71*, 2390–2396. https://doi.org/10.1093/jxb/eraa079.

11. Petricka, J.J., Winter, C.M., and Benfey, P.N. (2012). Control of *Arabidopsis* root development. Annu. Rev. Plant Biol. *63*, 563–590. https://doi.org/10.1146/annurev-arplant-042811-105501.

12. Mähönen, A.P., ten Tusscher, K., Siligato, R., Smetana, O., Díaz-Triviño, S., Salojärvi, J., Wachsman, G., Prasad, K., Heidstra, R., and Scheres, B. (2014). PLETHORA gradient formation mechanism separates auxin responses. Nature *515*, 125–129. https://doi.org/10.1038/nature13663.

13. Kuchen, E.E., Fox, S., de Reuille, P.B., Kennaway, R., Bensmihen, S., Avondo, J., Calder, G.M., Southam, P., Robinson, S., Bangham, A., and Coen, E. (2012). Generation of leaf shape through early patterns of growth and tissue polarity. Science *335*, 1092–1096. https://doi.org/10.1126/science.1214678.

14. Monniaux, M., Pieper, B., McKim, S.M., Routier-Kierzkowska, A.L., Kierzkowski, D., Smith, R.S., and Hay, A. (2018). The role of *APETALA1* in petal number robustness. eLife *7*, e39399. https://doi.org/10.7554/eLife.39399.

15. Zhang, Z., Runions, A., Mentink, R.A., Kierzkowski, D., Karady, M., Hashemi, B., Huijser, P., Strauss, S., Gan, X., Ljung, K., et al. (2020). A WOX/auxin biosynthesis module controls growth to shape leaf form. Curr. Biol. *30*, 4857–4868.e6. https://doi.org/10.1016/j.cub.2020.09.037.

16. Kierzkowski, D., Runions, A., Vuolo, F., Strauss, S., Lymbouridou, R., Routier-Kierzkowska, A.L., Wilson-Sánchez, D., Jenke, H., Galinha, C., Mosca, G., et al. (2019). A growth-based framework for leaf shape development and diversity. Cell *177*, 1405–1418.e17. https://doi.org/10.1016/j.cell.2019.05.011.

17. Sabatini, S., Heidstra, R., Wildwater, M., and Scheres, B. (2003). SCARECROW is involved in positioning the stem cell niche in the *Arabidopsis* root meristem. Genes Dev. *17*, 354–358. https://doi.org/10.1101/gad.252503.

18. Di Mambro, R., Sabatini, S., and Dello Ioio, R. (2018). Patterning the axes: a lesson from the root. Plants (Basel) *8*, 8. https://doi.org/10.3390/plants8010008.

19. Ivanov, V.B., and Dubrovsky, J.G. (2013). Longitudinal zonation pattern in plant roots: conflicts and solutions. Trends Plant Sci. *18*, 237–243. https://doi.org/10.1016/j.tplants.2012.10.002.

20. Swarup, R., Perry, P., Hagenbeek, D., Van Der Straeten, D., Beemster, G.T., Sandberg, G., Bhalerao, R., Ljung, K., and Bennett, M.J. (2007). Ethylene upregulates auxin biosynthesis in *Arabidopsis* seedlings to enhance inhibition of root cell elongation. Plant Cell *19*, 2186–2196. https://doi.org/10.1105/tpc.107.052100.

21. De Vos, D., Vissenberg, K., Broeckhove, J., and Beemster, G.T. (2014). Putting theory to the test: which regulatory mechanisms can drive realistic growth of a root? PLoS Comput. Biol. *10*, e1003910. https://doi.org/10.1371/journal.pcbi.1003910.

22. Dello Ioio, R., Linhares, F.S., Scacchi, E., Casamitjana-Martinez, E., Heidstra, R., Costantino, P., and Sabatini, S. (2007). Cytokinins determine *Arabidopsis* root-meristem size by controlling cell differentiation. Curr. Biol. *17*, 678–682. https://doi.org/10.1016/j.cub.2007.02.047.

23. Dello Ioio, R., Nakamura, K., Moubayidin, L., Perilli, S., Taniguchi, M., Morita, M.T., Aoyama, T., Costantino, P., and Sabatini, S. (2008). A genetic framework for the control of cell division and differentiation in the root meristem. Science *322*, 1380–1384. https://doi.org/10.1126/science.1164147.

24. Perilli, S., Di Mambro, R., and Sabatini, S. (2012). Growth and development of the root apical meristem. Curr. Opin. Plant Biol. *15*, 17–23. https://doi.org/10.1016/j.pbi.2011.10.006.

25. Houston, K., Tucker, M.R., Chowdhury, J., Shirley, N., and Little, A. (2016). The plant cell wall: a complex and dynamic structure as revealed by the responses of genes under stress conditions. Front. Plant Sci. *7*, 984. https://doi.org/10.3389/fpls.2016.00984.

26. Hamant, O., Heisler, M.G., Jönsson, H., Krupinski, P., Uyttewaal, M., Bokov, P., Corson, F., Sahlin, P., Boudaoud, A., Meyerowitz, E.M., et al. (2008). Developmental patterning by mechanical signals in *Arabidopsis*. Science *322*, 1650–1655. https://doi.org/10.1126/science.1165594.

27. Cosgrove, D.J. (2018). Diffuse growth of plant cell walls. Plant Physiol. *176*, 16–27. https://doi.org/10.1104/pp.17.01541.

28. Zhang, T., Tang, H., Vavylonis, D., and Cosgrove, D.J. (2019). Disentangling loosening from softening: insights into primary cell wall structure. Plant J. *100*, 1101–1117. https://doi.org/10.1111/tpj.14519.

29. Cosgrove, D.J. (2015). Plant expansins: diversity and interactions with plant cell walls. Curr. Opin. Plant Biol. *25*, 162–172. https://doi.org/10.1016/j.pbi.2015.05.014.

30. Kierzkowski, D., Nakayama, N., Routier-Kierzkowska, A.L., Weber, A., Bayer, E., Schorderet, M., Reinhardt, D., Kuhlemeier, C., and Smith, R.S. (2012). Elastic domains regulate growth and organogenesis in the plant shoot apical meristem. Science *335*, 1096–1099. https://doi.org/10.1126/science.1213100.

31. Jonsson, K., Lathe, R.S., Kierzkowski, D., Routier-Kierzkowska, A.L., Hamant, O., and Bhalerao, R.P. (2021). Mechanochemical feedback mediates tissue bending required for seedling emergence. Curr. Biol. *31*, 1154–1164.e3. https://doi.org/10.1016/j.cub.2020.12.016.

32. Bassel, G.W., Stamm, P., Mosca, G., Barbier de Reuille, P., Gibbs, D.J., Winter, R., Janka, A., Holdsworth, M.J., and Smith, R.S. (2014). Mechanical constraints imposed by 3D cellular geometry and arrangement modulate growth patterns in the *Arabidopsis* embryo. Proc. Natl. Acad. Sci. USA *111*, 8685–8690. https://doi.org/10.1073/pnas.1404616111.

33. Müller, B., and Sheen, J. (2008). Cytokinin and auxin interaction in root stem-cell specification during early embryogenesis. Nature *453*, 1094–1097. https://doi.org/10.1038/nature06943.

34. Ruzicka, K., Simásková, M., Duclercq, J., Petrásek, J., Zazímalová, E., Simon, S., Friml, J., Van Montagu, M.C., and Benková, E. (2009). Cytokinin regulates root meristem activity via modulation of the polar auxin transport. Proc. Natl. Acad. Sci. USA *106*, 4284–4289. https://doi.org/10.1073/pnas.0900060106.

35. Argyros, R.D., Mathews, D.E., Chiang, Y.H., Palmer, C.M., Thibault, D.M., Etheridge, N., Argyros, D.A., Mason, M.G., Kieber, J.J., and Schaller, G.E. (2008). Type B response regulators of *Arabidopsis* play key roles in cytokinin signaling and plant development. Plant Cell *20*, 2102–2116. https://doi.org/10.1105/tpc.108.059584.

36. Dello Ioio, R., Galinha, C., Fletcher, A.G., Grigg, S.P., Molnar, A., Willemsen, V., Scheres, B., Sabatini, S., Baulcombe, D., Maini, P.K., and Tsiantis, M. (2012). A PHABULOSA/cytokinin feedback loop controls root growth in *Arabidopsis*. Curr. Biol. *22*, 1699–1704. https://doi.org/10.1016/j.cub.2012.07.005.

37. Street, I.H., Mathews, D.E., Yamburkenko, M.V., Sorooshzadeh, A., John, R.T., Swarup, R., Bennett, M.J., Kieber, J.J., and Schaller, G.E. (2016). Cytokinin acts through the auxin influx carrier AUX1 to regulate cell elongation in the root. Development *143*, 3982–3993. https://doi.org/10.1242/dev.132035.

38. Rutten, J.P., and Ten Tusscher, K. (2019). *In silico* roots: room for growth. Trends Plant Sci. *24*, 250–262. https://doi.org/10.1016/j.tplants.2018.11.005.

39. Beemster, G.T., and Baskin, T.I. (1998). Analysis of cell division and elongation underlying the developmental acceleration of root growth in *Arabidopsis thaliana*. Plant Physiol. *116*, 1515–1526. https://doi.org/10.1104/pp.116.4.1515.

40. van der Weele, C.M., Jiang, H.S., Palaniappan, K.K., Ivanov, V.B., Palaniappan, K., and Baskin, T.I. (2003). A new algorithm for computational image analysis of deformable motion at high spatial and temporal resolution applied to root growth. Roughly uniform elongation in the meristem and also, after an abrupt acceleration, in the elongation zone. Plant Physiol. *132*, 1138–1148. https://doi.org/10.1104/pp.103.021345.

41. Iwamoto, A., Kondo, E., Fujihashi, H., and Sugiyama, M. (2013). Kinematic study of root elongation in *Arabidopsis thaliana* with a novel image-analysis program. J. Plant Res. *126*, 187–192. https://doi.org/10.1007/s10265-012-0523-5.

42. Di Mambro, R., De Ruvo, M., Pacifici, E., Salvi, E., Sozzani, R., Benfey, P.N., Busch, W., Novak, O., Ljung, K., Di Paola, L., et al. (2017). Auxin minimum triggers the developmental switch from cell division to cell differentiation in the *Arabidopsis* root. Proc. Natl. Acad. Sci. USA *114*, E7641–E7649. https://doi.org/10.1073/pnas.1705833114.

43. van den Berg, T., Yalamanchili, K., de Gernier, H., Santos Teixeira, J., Beeckman, T., Scheres, B., Willemsen, V., and Ten Tusscher, K. (2021). A reflux-and-growth mechanism explains oscillatory patterning of lateral root branching sites. Dev. Cell *56*, 2176–2191.e10. https://doi.org/10.1016/j.devcel.2021.07.005.

44. von Wangenheim, D., Hauschild, R., Fendrych, M., Barone, V., Benková, E., and Friml, J. (2017). Live tracking of moving samples in confocal microscopy for vertically grown roots. eLife *6*, e26792. https://doi.org/10.7554/eLife.26792.

45. Rahni, R., and Birnbaum, K.D. (2019). Week-long imaging of cell divisions in the Arabidopsis root meristem. Plant Methods *15*, 30. https://doi.org/10.1186/s13007-019-0417-9.

46. Geng, Y., Wu, R., Wee, C.W., Xie, F., Wei, X., Chan, P.M., Tham, C., Duan, L., and Dinneny, J.R. (2013). A spatio-temporal understanding of growth regulation during the salt stress response in *Arabidopsis*. Plant Cell *25*, 2132–2154. https://doi.org/10.1105/tpc.113.112896.

47. Barbier de Reuille, P., Routier-Kierzkowska, A.L., Kierzkowski, D., Bassel, G.W., Schüpbach, T., Tauriello, G., Bajpai, N., Strauss, S., Weber, A., Kiss, A., et al. (2015). MorphoGraphX: a platform for quantifying morphogenesis in 4D. eLife *4*, 05864. https://doi.org/10.7554/eLife.05864.

48. Leitão, N., Dangeville, P., Carter, R., and Charpentier, M. (2019). Nuclear calcium signatures are associated with root development. Nat. Commun. *10*, 4865. https://doi.org/10.1038/s41467-019-12845-8.

49. Sapala, A., and Smith, R.S. (2020). Osmotic treatment for quantifying cell wall elasticity in the sepal of *Arabidopsis thaliana*. Methods Mol. Biol. *2094*, 101–112. https://doi.org/10.1007/978-1-0716-0183-9_11.

50. Grossmann, G., Guo, W.J., Ehrhardt, D.W., Frommer, W.B., Sit, R.V., Quake, S.R., and Meier, M. (2011). The RootChip: an integrated microfluidic chip for plant science. Plant Cell *23*, 4234–4240. https://doi.org/10.1105/tpc.111.092577.

51. Denninger, P., Reichelt, A., Schmidt, V.A.F., Mehlhorn, D.G., Asseck, L.Y., Stanley, C.E., Keinath, N.F., Evers, J.F., Grefen, C., and Grossmann, G. (2019). Distinct RopGEFs successively drive polarization and outgrowth of root hairs. Curr. Biol. *29*, 1854–1865.e5. https://doi.org/10.1016/j.cub.2019.04.059.

52. Sapala, A., Runions, A., Routier-Kierzkowska, A.L., Das Gupta, M., Hong, L., Hofhuis, H., Verger, S., Mosca, G., Li, C.B., Hay, A., et al. (2018). Why plants make puzzle cells, and how their shape emerges. eLife *7*, e32794. https://doi.org/10.7554/eLife.32794.

53. Mosca, G., Sapala, A., Strauss, S., Routier-Kierzkowska, A.L., and Smith, R.S. (2017). On the micro-indentation of plant cells in a tissue context. Phys. Biol. *14*, 015003. https://doi.org/10.1088/1478-3975/aa5698.

54. Montenegro-Johnson, T.D., Stamm, P., Strauss, S., Topham, A.T., Tsagris, M., Wood, A.T., Smith, R.S., and Bassel, G.W. (2015). Digital single-cell analysis of plant organ development using 3DCellAtlas. Plant Cell *27*, 1018–1033. https://doi.org/10.1105/tpc.15.00175.

55. Anderson, C.T., and Kieber, J.J. (2020). Dynamic construction, perception, and remodeling of plant cell walls. Annu. Rev. Plant Biol. *71*, 39–69. https://doi.org/10.1146/annurev-arplant-081519-035846.

56. Montesinos, J.C., Abuzeineh, A., Kopf, A., Juanes-Garcia, A., Ötvös, K., Petrásek, J., Sixt, M., and Benková, E. (2020). Phytohormone cytokinin guides microtubule dynamics during cell progression from proliferative to differentiated stage. EMBO J. *39*, e104238. https://doi.org/10.15252/embj.2019104238.

57. Hofhuis, H., Moulton, D., Lessinnes, T., Routier-Kierzkowska, A.L., Bomphrey, R.J., Mosca, G., Reinhardt, H., Sarchet, P., Gan, X., Tsiantis,

M., et al. (2016). Morphomechanical innovation drives explosive seed dispersal. Cell *166*, 222–233. https://doi.org/10.1016/j.cell.2016.05.002.

58. Bennett, M.J., Marchant, A., Green, H.G., May, S.T., Ward, S.P., Millner, P.A., Walker, A.R., Schulz, B., and Feldmann, K.A. (1996). Arabidopsis AUX1 gene: a permease-like regulator of root gravitropism. Science *273*, 948–950. https://doi.org/10.1126/science.273.5277.948.

59. Marchant, A., Bhalerao, R., Casimiro, I., Eklöf, J., Casero, P.J., Bennett, M., and Sandberg, G. (2002). AUX1 promotes lateral root formation by facilitating indole-3-acetic acid distribution between sink and source tissues in the Arabidopsis seedling. Plant Cell *14*, 589–597. https://doi.org/10.1105/tpc.010354.

60. Swarup, R., Friml, J., Marchant, A., Ljung, K., Sandberg, G., Palme, K., and Bennett, M. (2001). Localization of the auxin permease AUX1 suggests two functionally distinct hormone transport pathways operate in the *Arabidopsis* root apex. Genes Dev. *15*, 2648–2653. https://doi.org/10.1101/gad.210501.

61. Muday, G.K. (2001). Auxins and tropisms. J. Plant Growth Regul. *20*, 226–243. https://doi.org/10.1007/s003440010027.

62. Liao, C.Y., Smet, W., Brunoud, G., Yoshida, S., Vernoux, T., and Weijers, D. (2015). Reporters for sensitive and quantitative measurement of auxin response. Nat. Methods *12*, 207–210. https://doi.org/10.1038/nmeth.3279.

63. Fridman, Y., Strauss, S., Horev, G., Ackerman-Lavert, M., Reiner-Benaim, A., Lane, B., Smith, R.S., and Savaldi-Goldstein, S. (2021). The root meristem is shaped by brassinosteroid control of cell geometry. Nat. Plants *7*, 1475–1484. https://doi.org/10.1038/s41477-021-01014-9.

64. Pavelescu, I., Vilarrasa-Blasi, J., Planas-Riverola, A., González-García, M.P., Caño-Delgado, A.I., and Ibañes, M. (2018). A Sizer model for cell differentiation in *Arabidopsis thaliana* root growth. Mol. Syst. Biol. *14*, e7687. https://doi.org/10.15252/msb.20177687.

65. Graeff, M., Rana, S., Marhava, P., Moret, B., and Hardtke, C.S. (2020). Local and systemic effects of brassinosteroid perception in developing phloem. Curr. Biol. *30*, 1626–1638.e3. https://doi.org/10.1016/j.cub.2020.02.029.

66. Graeff, M., Rana, S., Wendrich, J.R., Dorier, J., Eekhout, T., Aliaga Fandino, A.C., Guex, N., Bassel, G.W., De Rybel, B., and Hardtke, C.S. (2021). A single-cell morpho-transcriptomic map of brassinosteroid action in the *Arabidopsis* root. Mol. Plant *14*, 1985–1999. https://doi.org/10.1016/j.molp.2021.07.021.

67. Ackerman-Lavert, M., and Savaldi-Goldstein, S. (2020). Growth models from a brassinosteroid perspective. Curr. Opin. Plant Biol. *53*, 90–97. https://doi.org/10.1016/j.pbi.2019.10.008.

68. Vaseva, I.I., Qudeimat, E., Potuschak, T., Du, Y., Genschik, P., Vandenbussche, F., and Van Der Straeten, D. (2018). The plant hormone ethylene restricts *Arabidopsis* growth via the epidermis. Proc. Natl. Acad. Sci. USA *115*, E4130–E4139. https://doi.org/10.1073/pnas.1717649115.

69. Salvi, E., Rutten, J.P., Di Mambro, R., Polverari, L., Licursi, V., Negri, R., Dello Ioio, R., Sabatini, S., and Ten Tusscher, K. (2020). A self-organized PLT/Auxin/ARR-B network controls the dynamics of root zonation development in *Arabidopsis thaliana*. Dev. Cell *53*, 431–443.e23. https://doi.org/10.1016/j.devcel.2020.04.004.

70. Sugimoto, K., Williamson, R.E., and Wasteneys, G.O. (2000). New techniques enable comparative analysis of microtubule orientation, wall texture, and growth rate in intact roots of Arabidopsis. Plant Physiol. *124*, 1493–1506. https://doi.org/10.1104/pp.124.4.1493.

71. Wang, Y., Ji, Y., Fu, Y., and Guo, H. (2018). Ethylene-induced microtubule reorientation is essential for fast inhibition of root elongation in *Arabidopsis*. J. Integr. Plant Biol. *60*, 864–877. https://doi.org/10.1111/jipb.12666.

72. Zhang, Y., Yu, J., Wang, X., Durachko, D.M., Zhang, S., and Cosgrove, D.J. (2021). Molecular insights into the complex mechanics of plant epidermal cell walls. Science *372*, 706–711. https://doi.org/10.1126/science.abf2824.

73. Jasinski, S., Piazza, P., Craft, J., Hay, A., Woolley, L., Rieu, I., Phillips, A., Hedden, P., and Tsiantis, M. (2005). KNOX action in *Arabidopsis* is mediated by coordinate regulation of cytokinin and gibberellin activities. Curr. Biol. *15*, 1560–1565. https://doi.org/10.1016/j.cub.2005.07.023.

74. Skalák, J., Vercruyssen, L., Claeys, H., Hradilová, J., Černý, M., Novák, O., Plačková, L., Saiz-Fernández, I., Skaláková, P., Coppens, F., et al. (2019). Multifaceted activity of cytokinin in leaf development shapes its size and structure in Arabidopsis. Plant J. *97*, 805–824. https://doi.org/10.1111/tpj.14285.

75. Yanai, O., Shani, E., Dolezal, K., Tarkowski, P., Sablowski, R., Sandberg, G., Samach, A., and Ori, N. (2005). *Arabidopsis* KNOXI proteins activate cytokinin biosynthesis. Curr. Biol. *15*, 1566–1571. https://doi.org/10.1016/j.cub.2005.07.060.

76. Schindelin, J., Arganda-Carreras, I., Frise, E., Kaynig, V., Longair, M., Pietzsch, T., Preibisch, S., Rueden, C., Saalfeld, S., Schmid, B., et al. (2012). Fiji: an open-source platform for biological-image analysis. Nat. Methods *9*, 676–682.

77. Strauss, S., Sapala, A., Kierzkowski, D., and Smith, R.S. (2019). Quantifying plant growth and cell proliferation with MorphoGraphX. Methods Mol. Biol. *1992*, 269–290. https://doi.org/10.1007/978-1-4939-9469-4_18.

78. Lockhart, J.A. (1965). An analysis of irreversible plant cell elongation. J. Theor. Biol. *8*, 264–275. https://doi.org/10.1016/0022-5193(65)90077-9.

79. Coen, E., Kennaway, R., and Whitewoods, C. (2017). On genes and form. Development *144*, 4203–4213. https://doi.org/10.1242/dev.151910.

80. Goriely, A. (2017). The Mathematics and Mechanics of Biological Growth. Interdisciplinary Applied Mathematics (Springer).

81. Avery, G.S. (1933). Structure and development of the tobacco leaf. Am. J. Bot. *20*, 565–592. https://doi.org/10.1002/j.1537-2197.1933.tb08913.x.

82. Hejnowicz, Z., and Romberger, J.A. (1984). Growth tensor of plant organs. J. Theor. Biol. *110*, 93–114. https://doi.org/10.1016/S0022-5193(84)80017-X.

83. Fox, S., Southam, P., Pantin, F., Kennaway, R., Robinson, S., Castorina, G., Sánchez-Corrales, Y.E., Sablowski, R., Chan, J., Grieneisen, V., et al. (2018). Spatiotemporal coordination of cell division and growth during organ morphogenesis. PLoS Biol. *16*, e2005952. https://doi.org/10.1371/journal.pbio.2005952.

84. Weber, A., Braybrook, S., Huflejt, M., Mosca, G., Routier-Kierzkowska, A.L., and Smith, R.S. (2015). Measuring the mechanical properties of plant cells by combining micro-indentation with osmotic treatments. J. Exp. Bot. *66*, 3229–3241. https://doi.org/10.1093/jxb/erv135.

85. Vogler, H., Draeger, C., Weber, A., Felekis, D., Eichenberger, C., Routier-Kierzkowska, A.L., Boisson-Dernier, A., Ringli, C., Nelson, B.J., Smith, R.S., and Grossniklaus, U. (2013). The pollen tube: a soft shell with a hard core. Plant J. *73*, 617–627. https://doi.org/10.1111/tpj.12061.

STAR★METHODS

KEY RESOURCES TABLE

REAGENT or RESOURCE	SOURCE	IDENTIFIER
Experimental models: Organisms/strains		
A. thaliana: Columbia-0 (Col-0)	NASC	N60000
A. thaliana: *arr1-3 arr12-1* (*arr1arr12*)	Dello Ioio et al.[22] and Street et al.[37]	N/A
A. thaliana: *phb-1d*	Dello Ioio et al.[36]	N/A
A. thaliana: *aux1-10* (SALK_020355)	NASC	N520355
A. thaliana: *DR5v2::ntdTomato*	Liao et al.[62]	N/A
A. thaliana: *DR5v2::ntdTomato aux1-10*	This study	N/A
Chemicals, peptides, and recombinant proteins		
Propidium iodide (PI)	Sigma-Aldrich	25535-16-4
Murashige and Skoog (MS) medium	Duchefa	M0222
trans-Zeatin	Sigma-Aldrich	6025-81-6
NaCl	Roth	231-598-3
Critical commercial assays		
Lab-Tek chambered coverslips	Thermo Scientific Nunc	15536
Software and algorithms		
Fiji (version 1.53f51)	Schindelin et al.[76]	https://fiji.sc/
MorphoGraphX (version 2.0)	Barbier de Reuille et al.[47]	https://www.MorphoGraphX.org
MorphoMechanX	Bassel et al.,[32] Mosca et al.,[53] and Hofhuis et al.[57]	https://www.MorphoMechanX.org
Inflation Models for MorphoMechanX	This study	https://doi.org/10.5281/zenodo.5188426

RESOURCE AVAILABILITY

Lead contact
Further information and requests for resources and reagents should be directed to and will be fulfilled by lead contact, Miltos Tsiantis (tsiantis@mpipz.mpg.de).

Material availability
Transgenic *Arabidopsis* seeds used in this study are stored in the Tsiantis lab at the Max Planck Institute for Plant Breeding Research. All unique/stable reagents generated in this study are available from the lead contact with a completed Materials Transfer Agreement.

Data and code availability

- Experimental model organisms/strains are listed in the key resources table. Microscopy data reported in this paper will be shared by the lead contact upon request.
- For the computational simulation, the model source code and all templates before and after pressurization have been deposited at Zenodo and are publicly available as of the date of publication. DOIs are listed in the key resources table.
- Any additional information required to reanalyze the data reported in this paper is available from the lead contact upon request.

EXPERIMENTAL MODEL AND SUBJECT DETAILS

Plant materials and growth conditions
All transgenic plants were on the *A. thaliana* Col-0 background and are listed in the key resources table. For time-lapse experiments, plants were grown in either chambered coverslips or the RootChip, both previously described.[44,50] In chambered coverslips, seeds were surface sterilized by 20% DanKlorix bleach detergent for 10 min, washed 6 times with ddH$_2$O and sown on 1/2MS medium, pH 5.8, 1.8% agar. After 2 days at 4°C for stratification, they were cultivated in a growth incubator at 22/18°C in a 16/8h day/night cycle illuminated by Osram Tubes (L58W/77 and L58W/840) with an intensity of 100 μmol/m^2/s for 4 days. Then, seedlings were transferred to Lab-Tek chambered coverslips and a block of 1/2MS medium placed on top of the root with the cotyledons remaining free to the air. Plants were cultivated for an additional day before imaging. In the RootChip system, seeds were surface sterilized and

sown on top of 1cm-long plastic pipette tips filled with 1/2MS medium. The seed-containing tips were stratified at 4°C for 2 days and then transferred to a growth incubator at 22/18°C in a 16/8h day/night cycle for 4 days. Tips with seedlings were placed in the RootChip and incubated vertically for an additional day before imaging. To compare root morphology among different growth systems (Figure S1), we used an additional growth system, the agar plate, where roots were grown vertically on the surface of 1/2MS medium, pH 5.8, 1.8% agar; the other conditions used, were as those for the chambered coverslips system.

METHOD DETAILS

Hormonal and osmotic treatments

In the chambered coverslips system, 1μM *trans*-Zeatin (tZ) was applied on the medium block and roots were imaged after 24h treatment. In the RootChip system, microchannels in the RootChip were filled with liquid 1/2 MS medium containing *trans*-Zeatin and roots were imaged after 6h treatment. When testing cell-wall stiffness in the RootChip, roots were imaged before and after 5min osmotic solution (0.2M NaCl) treatment (Video S1).

Microscopy and image analysis with MorphoGraphX

Roots were stained with 0.01% propidium iodide (PI) and imaged using a confocal laser-scanning microscope (LSM 880; Carl Zeiss) with an LD LCI "Plan-Apochromat" 25x/0.8 Imm Corr objective. All confocal images were acquired by placing the sample horizontally while imaging. We verified in a control experiment that this method is not different to the vertical placement of the roots (Figure S4C).

After acquiring the time-lapse images, the confocal stacks (3000-5000x600-800x60-100, Z resolution 0.5-1μm) were first saved as TIFF files using Fiji and then loaded into MorphoGraphX (MGX) where adjacent image tiles were merged into a single stack to reconstruct the whole root tip and then processed following the standard pipeline to create curved-surface segmented (2.5D) meshes with a cell lineage labeling. In a first step, the signal of the root cap cells was erased following their 3D segmentation. Then a curved surface mesh was extracted using the edge detection process. Finally, the stack signal underneath the surface mesh was projected onto the mesh to make cell outlines visible for the segmentation. The meshes were then used to quantify the cell length increase or decrease between two time points and the cells' distance from the quiescent center (for details see the MGX user guide and Strauss et al.[77]).

Since growth is the increase in dimension/mass with the progress of time, it is a quantity that can be applied to any cell in any organism. In plants, this can only occur through changes in the cell wall in response to turgor.[78–80] Symplastic plant growth has been mathematically described in detail and is typically defined by means of the relative elemental rate of growth, a tensor quantity that can be computed for arbitrary spatial dimensions, in our case for longitudinal growth in the root in 1D.[81,82] For our purposes, we did not measure cell divisions, which could feedback to the cellular growth.[83]

The MGX 2.5D epidermal (surface) segmentation is representative of cellular growth quantifications along the longitudinal axis of the entire root as the different layers are tied together and their growth must be synchronized to avoid tearing. This assumption is consistent with the point made by De Vos et al. (2014)[21] by defining their "Uniform Longitudinal Strain Rule". To validate this hypothesis with our data, we attempted a segmentation of the cortex layer for one sample, to directly compare the growth profiles of the epidermal and cortex layers. Their growth profiles did not show differences beyond measuring noise (Figure S2B).

To accommodate root curvature, a manually placed Bezier curve, originating from the quiescent center, acted as the central organ axis. To quantify cell length, we implemented a custom process (Mesh/Cell Atlas 3D/Surface/Analyze Cells Bezier Line) that computes the difference between the vertices of a cell that are closest and farthest from the quiescent center with respect to the Bezier curve (similar to 3D Cell Atlas[54] but for surface meshes). Growth was then computed as the change in cell length. All plots were created by exporting the MGX quantification data to Microsoft Excel and R. To quantify the distance from the SGC to the quiescent center, either in number of epidermal cells or absolute distance (Figures 2C, S4B, and S4C), for each replicate, we binned the data of the cells based on their distance to the quiescent center. The bin with the highest growth value was considered the location of the SGC. In a few cases, we observed two or more bins with similar values where we averaged their distances. To quantify the signal abundance along the root vasculature in Figure 6, we implemented another custom MGX process (Stack/Analysis/Export Histogram Bezier). This process utilizes a manually placed Bezier line that originates from the quiescent center and is aligned with the central root axis. The Bezier line was then split into segments of equal length to create histogram bins, bin size=100μm. For each voxel in the image stack, its closest line segment was determined and the total signal per line segment was computed.

When analyzing the expression of the auxin response reporter line *DR5v2::ntdTomato*, we observed that a few samples showed a slightly different expression pattern compared to the rest (2/11 within WT background, 1/6 within *aux1-10* background). But this variation was not associated with the effect of cytokinin on *DR5v2::ntdTomato* expression (Figure 6), because an analysis without these outlier samples returned the same conclusion.

Computational simulations

All simulations were performed within the MorphoMechanX framework (www.MorphoMechanX.org),[32,53,57] a modeling platform based on MorphoGraphX (www.MorphoGraphX.org).[47] We used the Finite Element Method (FEM) to simulate the effect of turgor pressure on the elastic expansion of cells (see Video S2). Simulation templates were created using the methods described in[32] with the Cell Maker plugin. For our first simulation, we created templates of 3X3 blocks of cuboid cells with a width and depth of 16μm and length of a multiple (0.5x - 15x) of 16μm (see Figures 4A–4D). For the idealized cylindrical templates of Figure S3, we created a radially symmetric template of cells with cell lengths derived from actual measurements of WT roots. In these simulations,

cell width was kept constant and only the epidermal layer of cells was represented, leaving the cylinder hollow. The root template shown in Figure 4F reproduces an idealized template with epidermal cell length, width and depth as measured from real 3D-segmented roots. Moreover, we also measured the depth and width of cortex and endodermis cells to create a realistic 3D template of the root's outer layers. As we were mainly interested in the epidermis, we simplified the innermost layers and modeled pericycle and stele cells as a larger cylinder comprised of 4 large cells. Cell files and layers were arranged in a staggered pattern as occurs in real roots (Figure 4F). The cell wall was modeled by means of the finite element methods as made of membrane elements.[32,53,57] We adopted a Saint Venant-Kirchhoff material law, either isotropic in all directions, or with one direction reinforced by fibers (transversely isotropic material law[57]). To assign the fiber orientation, we aligned the root elongation axis with the z-axis and found the projection of a normalized vector parallel to the z axis along the element surface (with a tolerance of 0.5). If the projection was below the tolerance, isotropic material properties, given as the average between the two Young moduli, were assigned. Once the projection was obtained, fiber orientation was assigned orthogonal to such direction in the plane of the mesh element, so that fiber reinforcement resulted in the circumferential direction of periclinal walls (Figure S3D). The template meshes consisted of triangles with areas ranging from 5-10μm (average element length ~3μm). We did a mesh refinement test on the root template and found that the results were not qualitatively affected. The FEM convergence tolerance was set to 1e-4, where the convergence criterion was given by the mean of average force norm and maximal force norm. The simulation parameters adopted are reported in Table S1: the left column ("Isotropic") refers to the box, hollow cylinder and isotropic root simulations; the right column ("Anisotropic") refers to the anisotropic root simulation. The values chosen are average for plant cell tissues.[53,84,85] For the anisotropic root inflation, the Poisson's ratio used is 0.16, as a value of 0.3 created convergence difficulties. We tested both values for Poisson ratio in the isotropic case and found no qualitative differences in the results.

In our simulations, we noted boundary effects on the cell walls exposed to the rootward and shootward end of the template due to bulging.[32] Hence, cells with exposed longitudinal walls showed a much higher increase in relative length compared to other cells. To explore the influence of the boundary effect, we created two cylinders with cells of the same length with either shorter or longer cells (Figure S3C). Upon pressurization, boundary effects that affected the relative length change were restricted to the exposed first and last layer of cells at the start and end of the template. Hence, in all our simulations we excluded cells with exposed longitudinal side walls from the quantifications.

QUANTIFICATION AND STATISTICAL ANALYSIS

Statistical analysis was performed using R and ggplot2 in Figures 1F, 2B, 2C, 3B, 3D, 3F, 4E, 4G–4J, 5B–5D, 6B, S1B, S2, S3E–S3I, S4B, and S4C. Shaded regions in Figures 2B, 3D, and 5B represent standard deviation. The statistical tests that were used and the number of replicates that were analyzed have been indicated in figure legends. The significance threshold used was $P < 0.05$.